Numerical Simulation and Comparative Analysis of Earth Air Heat Exchanger Designs

Mustapha Merdassi*[ID], Mokhtar Aouissi[ID]

Mechanical Engineering Laboratory, Department of Mechanical Engineering, University of Amar Telidji, Laghouat 03000, Algeria

Corresponding Author Email: m.merdassi@lagh-univ.dz

ABSTRACT

This study compares the performance of serpentine and spiral Earth-Air Heat Exchanger (EAHE) designs using ANSYS Fluent for numerical simulations, under varying inlet temperatures, flow rates, and lengths. The models were validated against experimental data for the serpentine design and numerical results for the spiral design, confirming their accuracy. The simulations focused on outlet temperatures and pressure losses at depths of 2 and 3 meters. Results show that both designs achieve similar thermal performance, with minor differences in outlet temperatures and pressure losses. At a depth of 3 meters, both designs reach outlet temperatures within the comfort range, with the spiral design exhibiting lower pressure losses. For example, at an inlet temperature of 46.1°C and a flow rate of 130 m³/h, the serpentine EAHE achieves an outlet temperature of 30.21°C with a pressure loss of 77 Pa, while the spiral EAHE achieves 30.02°C with 61 Pa. While the serpentine design offers slightly better temperature reduction, it incurs higher pressure losses due to turbulence at 90° bends. These findings underscore the need to consider both thermal performance and pressure losses when selecting the optimal EAHE design, as both configurations demonstrate effectiveness in cooling under the studied conditions.

1. INTRODUCTION

With rising energy demand and pollution from fossil fuels, transitioning to renewable energy has become an obligation to protect public health, stabilize the climate, and support sustainable economic growth [1]. Recently, Algeria's electricity demand peaked at 19,500 MW on July 21, 2024 [2]. Identifying new energy sources is crucial to meet local needs and facilitate energy exports. Renewable energy presents a promising option, and investment in this sector has become increasingly profitable. With government support, many universities and institutions are focusing their research on solar power, wind energy, bioenergy, geothermal energy, and energy storage technologies.

Among renewable sources, geothermal energy is a clean option that relies on stable soil temperatures throughout the year. One technique used to exploit this energy is the Earth Air Heat Exchanger (EAHE), which transfers heat from the ground to air flowing through buried pipes, facilitating effective heat exchange between the air and soil.

Several studies have made significant contributions in this field for example:

de Andrade et al. [3] conducted a numerical study using CFD simulations in Viamão, Brazil, to evaluate the performance of a Horizontal Rectilinear Earth–air Heat Exchanger (EAHE) in a subtropical climate. They applied the constructal design method and TOPSIS to optimize duct geometries. The study showed that an elliptical duct with an aspect ratio of H/L=6.0 achieved a 16.4% improvement in

thermal performance for heating and 15.9% for cooling compared to the conventional circular duct. Experimental validation was not mentioned.

Hummood et al. [4] conducted a numerical study in Nasiriya, Iraq, utilizing computational fluid dynamics (CFD) to assess the effectiveness of EAHE for building heating and cooling. The study examined how soil thicknesses (0D to 6D) impact EAHE efficiency under varying pipe lengths and airflow velocities. Findings showed stable wall temperatures for soil thicknesses from 1D to 6D, but at higher speeds, wall temperature differed from soil temperature due to disturbed soil effects. The study recommends burying pipes at a 3-4 m depth in undisturbed soil for optimal performance, highlighting EAHE's potential to improve building energy efficiency.

Xiao and Li [5] conducted a study, evaluating the performance of Earth-Air Heat Exchangers (EAHE) using five pipe types: aluminum, stainless steel, PVC, corrugated, and perforated corrugated pipes. They found that corrugated pipes significantly enhanced heat transfer efficiency, reducing pipe length by up to 33.33% and offering the most cost-effective solution with a 15.89-year payback period. Although perforated pipes improved soil temperature recovery, they reduced heat exchange efficiency. The findings highlight corrugated pipes as the most suitable for EAHE systems, promoting energy-efficient solutions.

Molina-Rodea et al. [6] examined the performance of a "U" type EAHE in Morelos, Mexico, installed in a compact 3 m² area with vertical wells less than 3 m deep. Conducted in

March with ambient temperatures reaching 35°C, the system achieved air temperature drops of 5.1-9.4°C and a maximum COP of 12.8. Over 70% of the heat exchange occurred in the first well, while the last well contributed minimally. The system demonstrated suitability for cooling urban offices with space constraints, though design improvements are needed for greater efficiency. Its compact design offers potential for use in urban and low-income settings.

Mostafaeipour et al. [7] investigated the energy performance and cost-effectiveness of EAHE's in a residential building in Kerman, Iran, a hot-dry climate. The study analyzes 9 different EAHE configurations with varying pipe lengths (25, 50, and 75 meters) and burial depths (1, 2, and 3 meters). The results demonstrate that EAHE systems can effectively reduce cooling and heating loads, saving up to 4% in cooling energy and 4% in heating energy annually. The study also highlights the economic viability of EAHE systems, with a payback period ranging from 3 to 16 years depending on the system configuration. The findings suggest that longer pipe lengths and deeper burial depths increase the system's efficiency, with the 50-meter and 75-meter systems showing substantial energy savings and shorter payback periods.

Zajch et al. [8] conducted a climate-based study to evaluate EAHE suitability across 273 sites in the Americas, considering both historical and projected climate conditions (RCPs from CMIP5). The analysis revealed that cooler climates will retain their ability to provide cooling despite rising cooling demands, while warmer climates will experience reduced EAHE suitability due to increased cooling needs. The findings highlight the importance of considering regional climate conditions and suggest that temperate climates should continue to prioritize EAHE systems for both heating and cooling in the face of climate change.

Nettari et al. [9] conducted a numerical study in southern Algeria using CFD to evaluate EAHE performance for cooling in arid climates. They found that a 3meter burial depth optimized cooling efficiency, with Ouargla achieving a higher thermal range (up to 22.5°C) compared to Ghardaïa (20°C), indicating greater suitability for EAHE systems in this region.

Sakhri et al. [10] conducted an experimental study in Béchar city, Algeria, using wind towers and Earth-to-Air Heat Exchangers (EAHE) to optimize indoor thermal comfort. They found that the open-window scenario improved thermal comfort by 50%, while the closed-window scenario showed an 18.75% improvement. The study demonstrates that combining wind towers with EAHEs can significantly enhance thermal comfort and reduce energy demands by at least half during summer and winter.

Roger et al. [11] conducted an experimental study in Cameroon to examine heat transfer in a bioclimatic Earth-Air Heat Exchanger (EAHE) model. Using a reduced-scale copper pipe buried in sand, they varied air speeds (1.2 to 2.9 m/s) and soil temperatures. Results showed that as air speed increased, the temperature difference between inlet and outlet air rose by 0.653°C per unit of air speed, and the heat transfer coefficient increased by 1.369 W/m²K. The study highlighted that higher air speeds enhance heat exchange efficiency in EAHE systems.

Ahmad et al. [12] optimized an Earth-Air Tube Heat Exchanger (EATHE) system for cooling applications using the Taguchi method. Analyzing six factors—installation depth, pipe diameter, pipe material conductivity, inlet air temperature, outlet air temperature, and air velocity,they found that pipe diameter was the most influential factor, contributing 69.12% to ground heat exchanger length and 75.97% to heat transfer

coefficient. The study identified optimal parameter combinations, achieving a minimum ground heat exchanger length of 6.44 m and maximum heat transfer coefficient of 130.67 W/m²K, demonstrating significant efficiency improvements for cooling systems.

Moummi et al. [13] evaluated an EAHE system with a serpentine design for cooling in Biskra city, Algeria, through theoretical modeling and experimentation. They found a significant temperature drop of up to 15°C from inlet to outlet, highlighting the system's potential for geothermal cooling. The study demonstrates the EAHE's effectiveness in reducing air temperature and energy consumption for building climate control in varied Algerian climates.

Benrachi et al. [14] used Ansys Fluent to study a new EAHE with a spiral design for hot, arid climates in El Oued City, Algeria. Increasing pitch spacing from 0.2 to 2 m improved efficiency, reducing outlet air temperature by 6°C. However, increasing airflow velocity from 2 to 5 m/s decreased mean efficiency from 60% to 33% and COP from 2.84 to 0.46. The study highlights the importance of optimizing design parameters for enhanced EAHE performance.

Belloufi et al. [15] studied the transient behavior of a continuously operating EAHE in Biskra, Algeria, using a 3-meter-deep PVC pipe. Their results, based on experiments and simulations, showed a maximum temperature drop of 18.06°C and a thermal efficiency of 78.96%, highlighting the influence of soil thermal conductivity and the primary cooling effect within the first 30 meters of the pipe.

Moreover, various studies highlight the effectiveness of EAHEs for enhancing thermal performance. Sehli et al. [16] found that an air-to-ground exchanger in Béchar city, Algeria, achieved an outlet temperature of 24°C with a length to diameter ratio of 250 and stable ground temperatures around 21°C. Hacini et al. [17] and Hadjadj et al. [18] emphasized optimizing parameters for cooling efficiency in different Algerian climates. Xamán et al. [19] demonstrated that thermal insulation significantly improved EAHE performance in moderate and humid-hot regions, underscoring the systems' potential for energy efficiency and thermal comfort, Congedo et al. [20] assessed a horizontal air-ground heat exchanger (HAGHE) in a Mediterranean climate using a CFD model, reporting a cooling effect of 2-3°C in summer and humidity below 60%. They noted occasional winter reverse thermal flow, recommending a bypass, with optimal performance at 5 meters depth and 3 W/(mK) conductivity, making the system suitable for nearly zero energy buildings (nZEBs).

All the aforementioned studies focus on analyzing the performance of Earth-Air Heat Exchangers (EAHEs) under different geographic, climatic, and operational conditions. They examine the influence of various design and environmental parameters, such as pipe depth, length, material, airflow velocity, burial configurations, and soil properties, to optimize thermal efficiency and energy savings.

Building on this foundation the present paper aims to analyze the performance of two Earth-Air Heat Exchanger (EAHE) designs specifically, a serpentine configuration and a spiral configuration, both of equal length through numerical simulation. The simulation model will be validated against experimental data from Moummi et al. [13] for the serpentine design and against the numerical results of Benrachi et al. [14] for the spiral design. Using local climatic data from Laghouat City, Algeria, we will assess the performance of both designs while varying several parameters, including length, depth, and airflow rate. ANSYS Fluent will be utilized as the

Computational Fluid Dynamics (CFD) tool for this study.

The paper is organized into four sections: "Comprehending EAHEs" covers their principles, "EAHE Modeling" explains the methodology, and "Results and Discussion" assesses performance under Laghouat's climate for optimization. Finally, the conclusion summarizes the key findings and provides recommendations.

2. COMPREHENDING EARTH AIR HEAT EXCHANGERS

The ground's stable temperatures offer significant potential for Earth-Air Heat Exchanger (EAHE) systems to reduce heating and cooling needs. In Laghouat City, Algeria (32°N, ~750 m), the ground temperature is more moderate than ambient air, Figures 1 and 2 represent the mean ambient temperature [21] versus ground temperature at a depth of 3 meters (calculated by Eq. (2)) for January and August 2023. It is evident that ground temperatures are higher in winter and lower in summer, highlighting EAHE's effectiveness. EAHE systems work by passing air through underground ducts, where it exchanges heat with the earth's stable temperature, heating the air in winter and cooling it in summer, reducing the need for conventional heating and cooling methods.
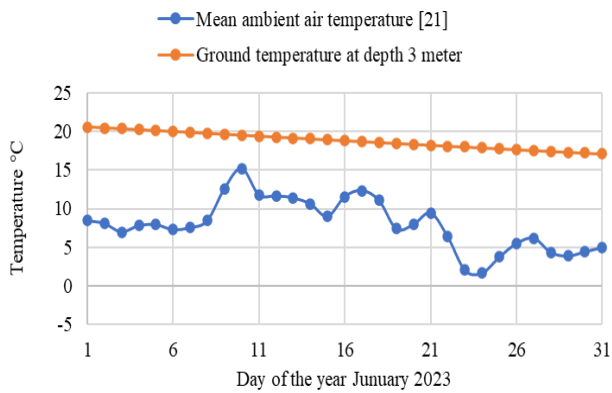
Figure 1. Mean ambient air vs. ground temperature at a depth of 3 meters for January 2023, Laghouat City, Algeria
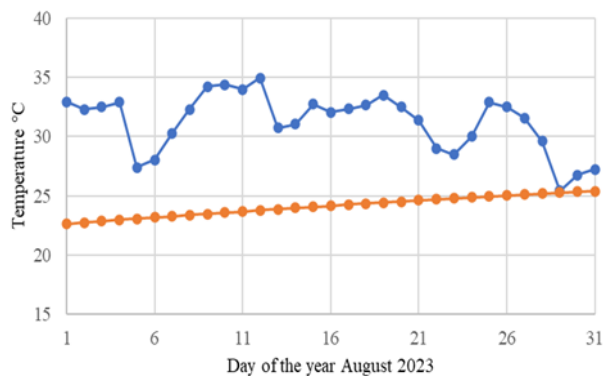

Figure 2. Mean ambient air vs. ground temperature at a depth of 3 meters for August 2023, Laghouat City, Algeria

3. EAHE MODELING

The modeling in this study is carried out using the CFD platform ANSYS Fluent, with a structured approach that includes mathematical modeling, geometric configuration, and mesh generation. The mathematical modeling includes soil temperature modeling to predict heat exchange conditions and airflow modeling through the EAHE, ANSYS Fluent is a comprehensive computational fluid dynamics (CFD) software that uses finite volume methods to solve fluid flow and heat transfer problems by dividing complex geometries into small control volumes.

Figure 3 illustrates a flowchart of the steps involved in using ANSYS Fluent for this simulation process.
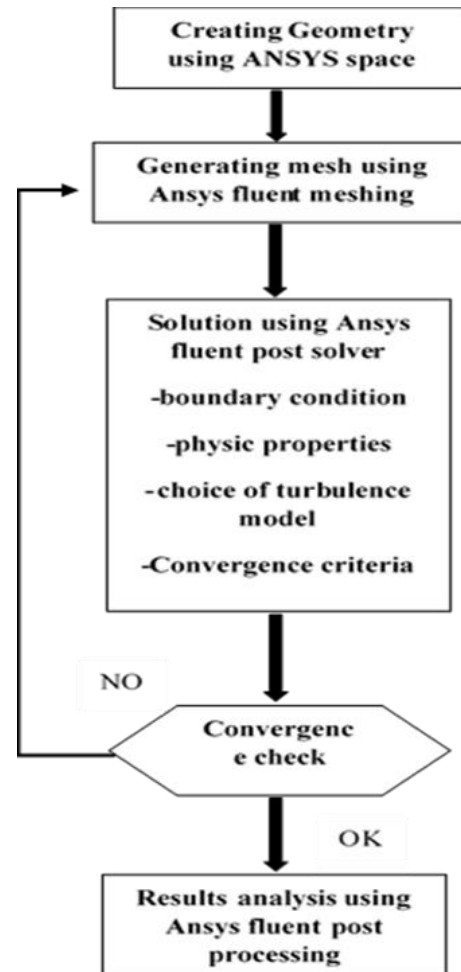
Figure 3. Ansys fluent flowchart

3.1 The soil temperature modelling

The heat conduction equation in one dimension (assuming heat transfer only in the vertical direction) is given by:

$$\frac{\partial^2 T}{\partial z^2} = \frac{1}{\propto}\frac{\partial T}{\partial t} \tag{1}$$

Taking into consideration that the soil is considered a homogeneous medium with constant thermophysical properties (ρ, μ, k, Cp) for the soil, the solution of Eq. (1) is given by Kusuda et al. [22]:

$$T_{soil}(z,t) = -T_{amp}e^{\left(-z\sqrt{\frac{\pi}{365*\alpha s}}\right)}$$
$$\times cos(\frac{2\pi}{365}(t - t_0 - \frac{z}{2}\sqrt{\frac{365}{\pi*\alpha s}})) \tag{2}$$

where,
- $T_{soil}(z, t)$ is the soil temperature at depth z and time t (°C).
- T_{mean} is the mean annual temperature calculated as follows (°C):

$$T_{mean} = \frac{T_{max} + T_{min}}{2} \qquad (3)$$

- T_{max} and T_{min} are the maximum and minimum ambient temperatures (°C).
- T_{amp} is the amplitude of the temperature calculated as follows (°C):

$$T_{amp} = \frac{T_{max} - T_{min}}{2} \qquad (4)$$

- t_0 is the time of year (day) when the surface temperature is highest.
- α_s is the thermal diffusivity of the soil (m²/s).

3.2 The air flow modelling through the EAHE

Airflow modelling through EAHE is crucial for evaluating their performance and efficiency. Considering the air is incompressible with constant physical properties and the flow is turbulent, with the k-ε model chosen, the process is governed by the following equations [23]:

Mass equation:

$$\frac{\partial \rho}{\partial t} + \frac{\partial U_i}{\partial x_i} = 0 \qquad (5)$$

Momentum equation:

$$U_j \frac{\partial U_i}{\partial x_j} = -\frac{1}{\rho} \frac{\partial P}{\partial x_i} + \vartheta \frac{\partial^2 U_i}{\partial x_j \partial x_j} \qquad (6)$$

Momentum equation:

$$U_j \frac{\partial T}{\partial x_j} = \frac{1}{\rho C_p} \left(\frac{\lambda \partial^2 T}{\partial x_j \partial x_j} + \phi \right) \qquad (7)$$

Turbulence kinetic energy equation:

$$\frac{\partial}{\partial x_i} (\rho K U_i) = \frac{\partial}{\partial x_j} \left[\left(\mu + \frac{\mu_t}{\sigma_k} \right) \frac{\partial K}{\partial x_j} \right] + G_k + \rho \varepsilon \qquad (8)$$

Specific dissipation rate equation:

$$\frac{\partial}{\partial t} (\rho \varepsilon) + \frac{\partial}{\partial x_i} (\rho \varepsilon U_i)$$
$$= \frac{\partial}{\partial x_j} \left[\left(\mu + \frac{\mu_t}{\sigma_\varepsilon} \right) \frac{\partial \varepsilon}{\partial x_j} \right] + C_1 \frac{\varepsilon}{K} (G_k) \qquad (9)$$
$$- C_2 \rho \frac{\varepsilon^2}{K}$$

where, the turbulent viscosity μ_t and the production rate G_k are determined by:

$$\mu_t = C_\mu \rho \frac{K^2}{\varepsilon} \qquad (10)$$

$$G_K = \mu_t \frac{\partial U_i}{\partial x_j} \left(\frac{\partial U_i}{\partial x_j} + \frac{\partial U_j}{\partial x_i} \right) \qquad (11)$$

The closure coefficients are given as follows:

$C_1 = 1.44$, $C_2 = 1.92$, $\alpha_k = 1.0$, $\alpha_\varepsilon = 1.3$, $C_\mu = 0.09$.

3.2.1 Pressure loss

Pressure loss values, ΔP, of air through the EAHE can be expressed:

$$\Delta P = \Delta P_f + \Delta P_s \qquad (12)$$

where, ΔP_f is frictional pressure losses and is given by:

$$\Delta P_f = f \frac{L}{D} \frac{\rho V^2}{2} \qquad (13)$$

where,
- ΔP = frictional pressure loss (Pa).
- f = Darcy-Weisbach friction factor (dimensionless).
- L = length of the pipe or duct (m).
- D = hydraulic diameter of the pipe or duct (m).
- ρ = density of the fluid (kg/m³).
- V = flow velocity of the fluid (m/s).

And ΔP_s is singular pressure losses and is given by:

$$\Delta P_s = K \frac{\rho V^2}{2} \qquad (14)$$

where,
- ΔP_5 = singular (or minor) pressure loss (Pa).
- K = loss coefficient (dimensionless), specific to the type of fitting, bend, valve, etc.

3.3 EAHE design configurations and mesh generation

The two EAHE designs utilized in our numerical simulations were developed using the ANSYS Fluent geometric tool. Figures 4 and 5 illustrate each design: Figure 4 depicts a serpentine EAHE, and Figure 5 depicts a spiral EAHE.
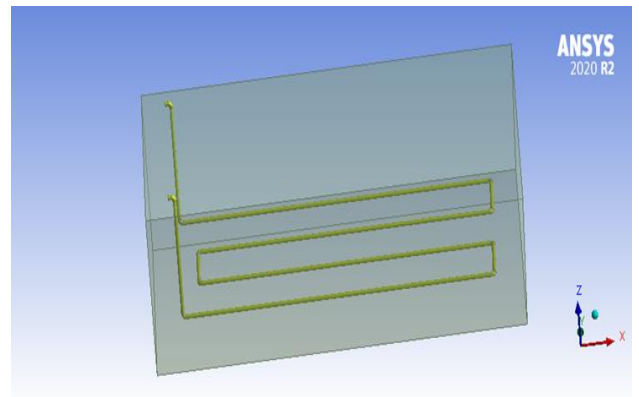
Figure 4. Geometry of the serpentine EAHE

The geometries of the EAHE designs are meshed using ANSYS Fluent's meshing tool, employing an unstructured tetrahedral mesh with refinement near the walls. Figures 6 and 7 show the meshing configurations for the serpentine and
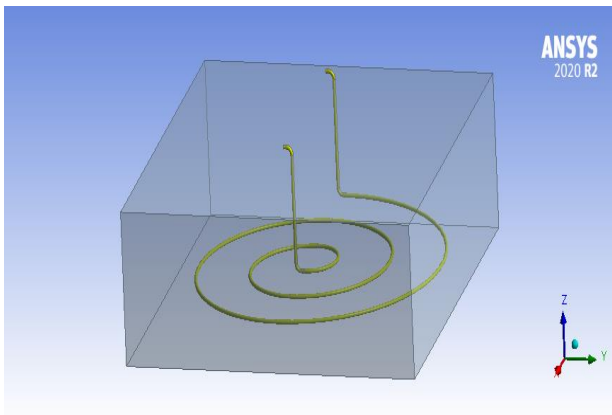
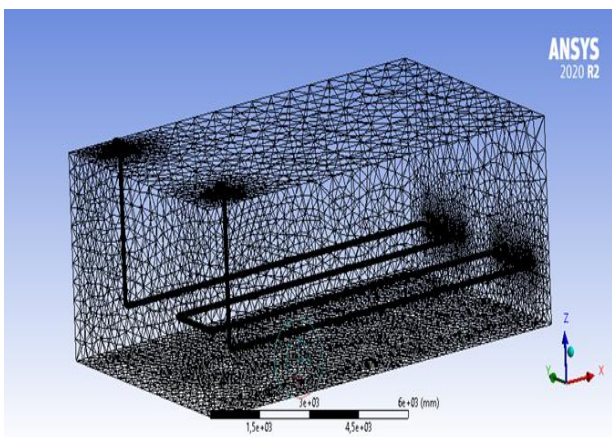spiral systems, respectively.

Figure 5. Geometry of the spiral

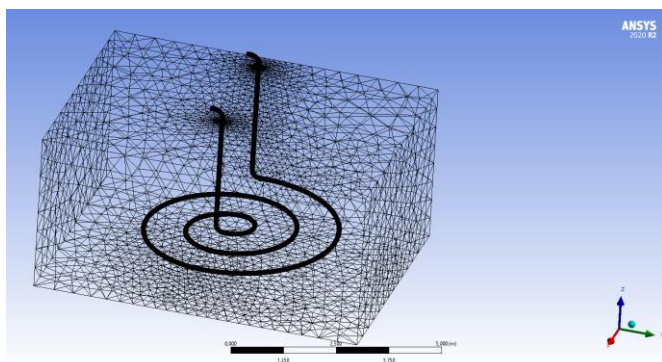**Figure 6.** Meshing of EAHE system: Serpentine design

Figure 7. Meshing of EAHE system: Spiral design

3.4 Boundary conditions

The model was defined using the following boundary conditions (Figure 8).

3.4.1 Inlet conditions
At the inlet of the channel, the air temperature corresponds to the ambient air temperature (based on climatic conditions), and the inlet flow rate remains constant throughout its passage through the EAHE.

3.4.2 Outlet conditions
At the outlet, the pressure was set equal to the atmospheric pressure.

3.4.3 Pipe's wall condition
The pipe walls are in direct contact with the surrounding soil, and the initial temperature of the pipe is determined by the soil temperature at the corresponding depth.
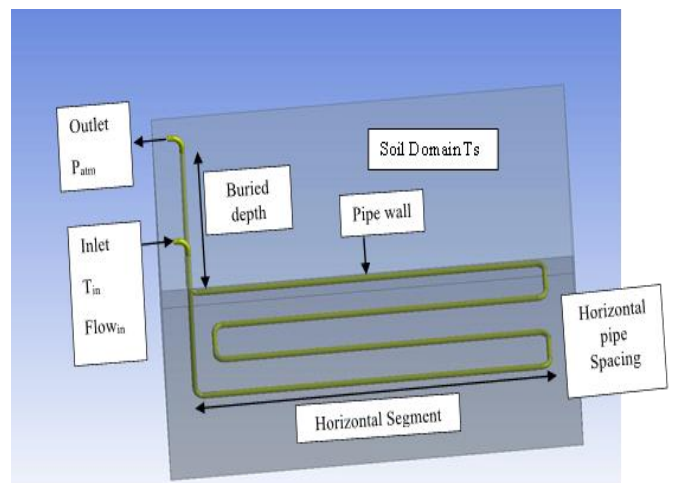

Figure 8. Boundary conditions

4. RESULTS AND DISCUSSION

4.1 Serpentine numerical model validation

Before evaluating the two EAHE designs under the local climatic conditions of Laghouat, Algeria, we must first validate our numerical model against the experimental data obtained by Moummi et al. [13]. The design to be validated, shown in Figure 4, is identical to the one used in the experimental study, featuring a total EAHE length of 45.7 meters and a horizontal pipe spacing of 2 meters. Table 1 presents the properties of the soil, PVC pipe, and air used in the experiment [13].

Table 1. Soil, pipe, and air properties used in the experiment [13]

Parameters	Value
Soil thermal conductivity λ_S	2.01 [Wm^{-1}°C^{-1}]
Soil thermal specific heat C_s	1380 [Jkg^{-1}°C^{-1}]
Soil density ρ_s	2300 [kg m^{-3}]
T_{soil} at z=3 m	24 [°C]
Pipe thermal conductivity λ_p	0.17 [Wm^{-1}°C^{-1}]
Pipe thermal conductivity λ_p	1.17 [Wm^{-1}°C^{-1}]
Pipe thermal specific heat C_p	900 [Jkg^{-1}°C^{-1}]
Pipe diameter D	0.11 [m]
Pipe outer-diameter D_{out}	0.115 [m]
Pipe buried dept z	3 [m]
Air volume rate Q_v	130, 155 [m^{3}h^{-1}]
Air thermal specific heat C_a	1000 [Jkg^{-1}°C^{-1}]
Air inlet temperature T_a	36.5 [°C]

Table 2 summarizes the various parameters used in the simulation calculations, including fluid type, flow regime, selected turbulence model, number of iterations, as well as the boundary and initial conditions.

To determine the effect of mesh size, we will evaluate the numerical model using two different cases, as shown in Table 3.

Figure 9 represents a comparison of air temperature along the EAHE with serpentine design for the two cases and the

experimental data, confirming the reliability of our numerical simulation for predicting the performance of the serpentine design. The numerical results align well with the experimental data, with no significant difference in accuracy between the meshes and the experimental results.

Table 2. Simulation parameters and conditions

Flow Regime	Turbulent
Turbulence model	K-ε
Fluid	Air
Pipe	PVC
Mesh type	tetrahedral
Inlet conditions	T_{inlet}=36.5°C $Flow_{inlet}$=130, 155 m³/h
Outlet conditions	P=P_{atm}
Maximum number of iterations	1000
Convergence error	10^6

Table 3. Cases of meshing used in numerical calculation (serpentine EAHE)

Cases	Element Number	Nodes Number
Case 1	4389988	7044361
Case 2	3382442	5415423
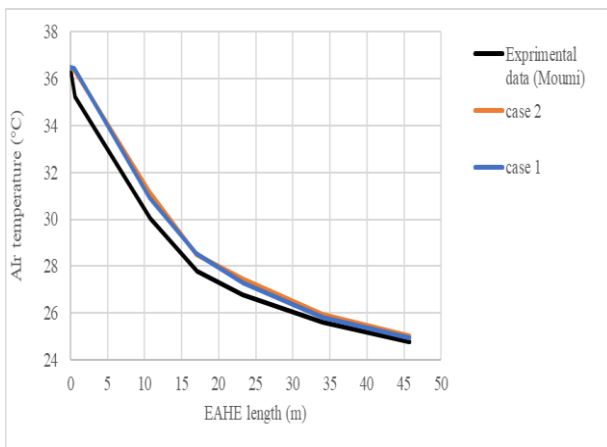
Figure 9. Comparison of air temperature along the EAHE of the two cases and experimental data [13]

Table 4. Soil, pipe, and air properties used in the numerical study [14]

Parameters	Value
Soil thermal conductivity λ_S	2.1 [Wm^{-1}°C^{-1}]
Soil thermal specific heat C_s	1780 [Jkg^{-1}°C^{-1}]
Soil density ρ_s	1800 [kg m^{-3}]
T_{soil} at z=3 m	27 [°C]
Pipe thermal conductivity λ_p	0.17 [Wm^{-1}°C^{-1}]
Pipe thermal conductivity λ_p	1.17 [Wm^{-1}°C^{-1}]
Pipe thermal specific heat C_p	900 [Jkg^{-1}°C^{-1}]
Pipe diameter D	0.1 [m]
Pipe buried dept z	3 [m]
Inlet velocity	2 [ms^{-1}]
Air thermal specific heat C_a	1010 [Jkg^{-1}°C^{-1}]
Air inlet temperature T_a	47.15 [°C]

4.2 Spiral numerical model validation

The spiral numerical model (Figure 2) will be validated against the numerical results conducted by Benarchi et al. [14], which involve a pipe length of 25.77 m and a pitch (Pt) of 2 m.

Table 4 presents the properties of the soil, PVC pipe, and air used in the numercial study [14].

Table 5 summarizes the various parameters used in the simulation calculations.

**Table 5.** Simulation parameters and conditions (spiral design)

Flow Regime	Turbulent
Turbulence model	K-ε
Fluid	Air
Pipe	PVC
Mesh type	Tetrahedral
Inlet conditions	T_{inlet}=47.15°C V_{inlet}=2 m/s
Outlet conditions	P=P_{atm}
Maximum number of iterations	1000
Convergence error	10^6

To examine the effect of mesh size, the numerical model of the spiral EAHE will be evaluated using two different cases, as presented in Table 6.

Table 6. Cases of meshing used in numerical calculation (spiral EAHE)

Cases	Element Number	Nodes Number
Case 1	3652785	5638374
Case 2	5012364	7256981

Figure 10 presents a comparison of air temperature along the EAHE with a spiral design between the previous numerical study [9] and the present work's numerical results for the two cases of mesh sizing. A strong agreement is observed between the two, demonstrating the reliability of our numerical model for the spiral design.
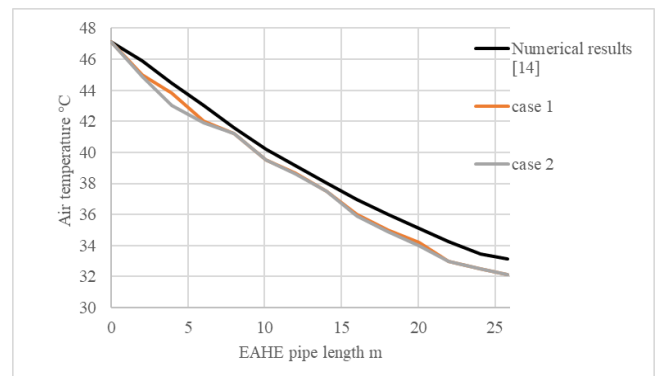
Figure 10. Comparison of air temperature along the EAHE between the previous numerical study [14] and the present work's numerical results

The validation of both EAHE designs in this study, considering different mesh scenarios, aligns with findings from previous research. Hummood et al. [4] demonstrated the accuracy of CFD models with minimal air temperature variations across three mesh cases, while de Andrade et al. [3] observed negligible differences in computational time across four mesh configurations, supporting the use of the default mesh.

Building on the validation of both designs, we will now evaluate the two designs under the climatic conditions of

Laghouat City, Algeria, using numerical simulations with ANSYS Fluent.

4.3 Evaluation of EAHE designs

To evaluate EAHE designs effectively using local climatic data, predicting the soil temperature is essential. Figure 11 shows the soil temperature at three depths of 1, 2 and 3 meters, throughout 2023 in Laghouat City. It highlights how the temperature changes with depth and time over the year, considering the soil properties as detailed in Table 1, and the climatic data from the year 2023 [21] was employed for these calculations, using Eq. (2).
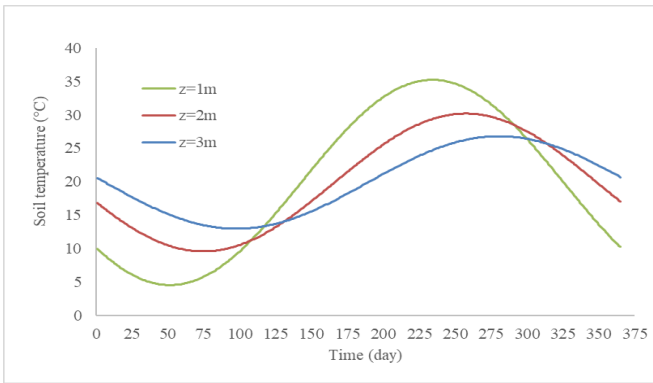
Figure 11. Yearly variation of soil temperature at different depths

To evaluate the two designs of the EAHE, July 2023 was selected as a case study due to the highest recorded temperature of the year on the 30th, reaching 46.1℃ [21]. According to Figure 11, the soil temperatures on July 30 at depths of 1, 2, and 3 meters were 35℃, 28℃, and 23℃, respectively. Given that the ambient air temperature on this day was 46.1℃, it is evident that a depth of 1 meter does not provide a sufficient temperature differential for effective cooling. Therefore, evaluating the EAHE designs at depths of 2 and 3 meters is more appropriate, where the lower soil temperatures offer better potential for heat exchange.

For these evaluations, EAHE lengths of 49 and 50 meters were selected at depths of 2 and 3 meters, respectively, ensuring sufficient length to optimize heat transfer. This analysis considers the numerical conditions detailed in Table 2 and the physical properties outlined in Table 3, with an initial air temperature of 46.2℃. The spacing between the horizontal pipes of the EAHE is 2 meters for both designs. Figures 12 and 13 present the air temperature contours along the EAHE for the two designs at a depth of 2 meters.

Figures 12 and 13 effectively illustrate how the soil acts as a cooling source for the air as it flows through the EAHE in both designs. The interaction between the air and the surrounding soil is clearly depicted through the colour gradients representing temperature variations along the EAHE and the adjacent soil.

To compare the performance of serpentine and spiral EAHE designs at a depth of 2 meters, with an inlet temperature of 46.1℃ and flow rates of 130, 200, and 250 m³/h, the following figures illustrate the air temperature distribution along the EAHE for each design and the pressure losses for both designs at each flow rate.
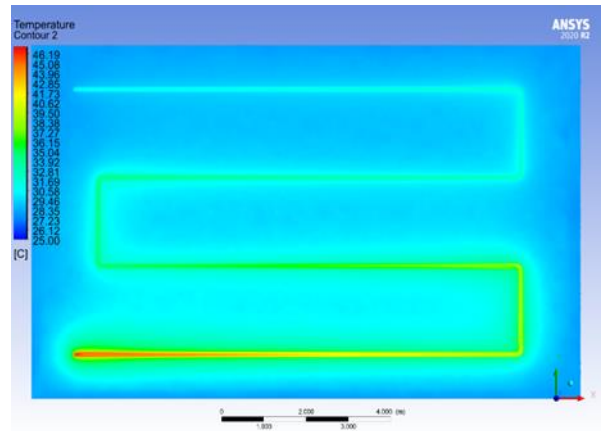

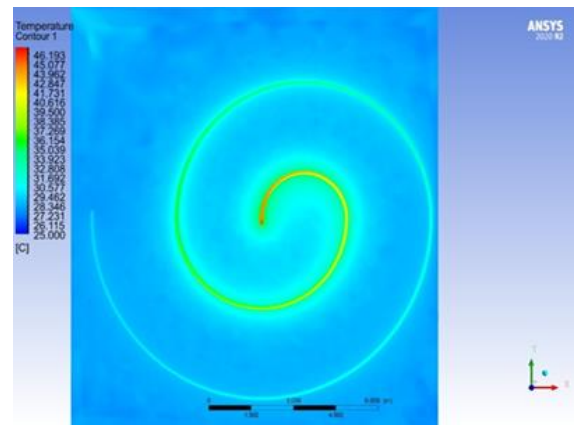**Figure 12.** Isothermal contours of soil and spiral EAHE horizontal path at 2 m depth

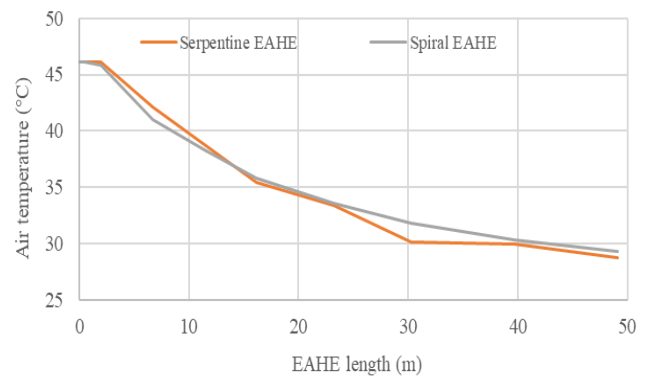**Figure 13.** Isothermal contours of soil and spiral EAHE horizontal path at 2 m depth

Figure 14. Air temperature throughout the EAHE for two designs (flow rate =130 m³/h)

For a total length of 49 meters at a depth of 2 meters, the results demonstrate the performance differences between the serpentine and spiral EAHE designs under varying flow rates. At a flow rate of 130 m³/h, the serpentine design achieves a lower outlet temperature (28.37℃) compared to the spiral design (29.39℃, Figure 14), but this is accompanied by a higher-pressure loss (124.10 Pa versus 101.11 Pa, Figure 15). As the flow rate increases to 200 m³/h and 250 m³/h (Figure 16 and Figure 17), both designs show a rise in outlet temperature, with the serpentine EAHE maintaining slightly better cooling performance (29.95℃ and 30.66℃, respectively) than the spiral EAHE (30.45℃ and 31.25℃,

respectively). However, the serpentine design consistently incurs higher pressure losses, reaching 405 Pa at 250 m³/h compared to 323 Pa for the spiral design (Figure 18 and Figure 19). These figures highlight the trade-off between thermal performance and pressure loss, showing that the serpentine design offers slightly better cooling efficiency but at the expense of higher-pressure losses.
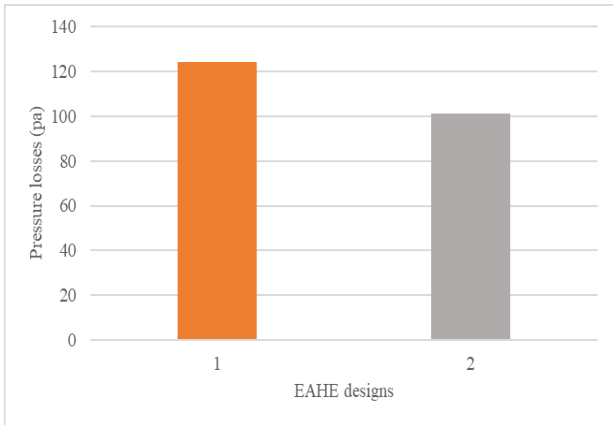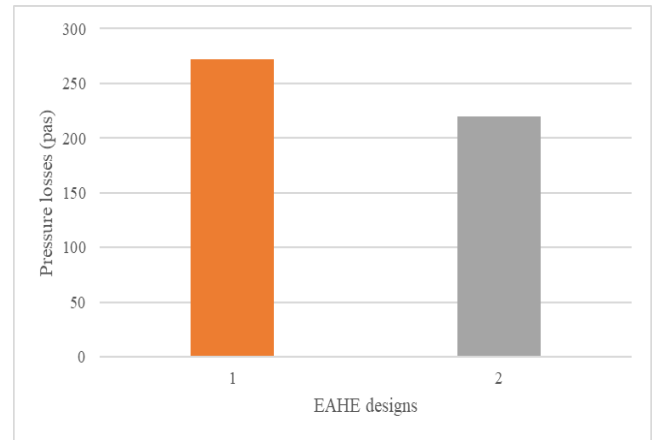

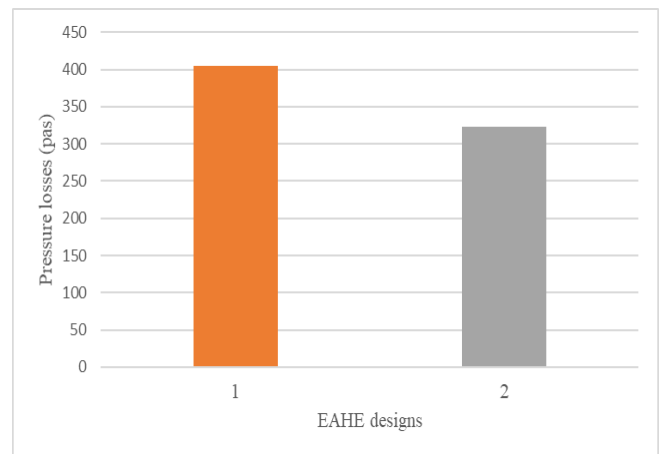**Figure 15.** Pressure losses throughout the EAHE designs (flow rate =130 m³/h)
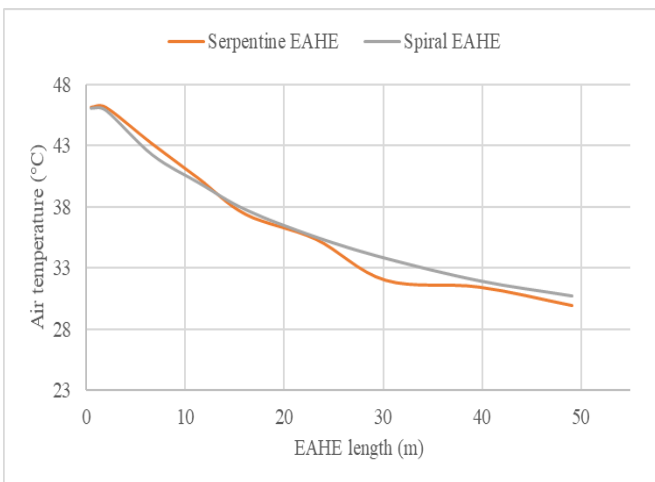
Figure 16. Air temperature throughout the EAHE for two designs (flow rate =200 m³/h)
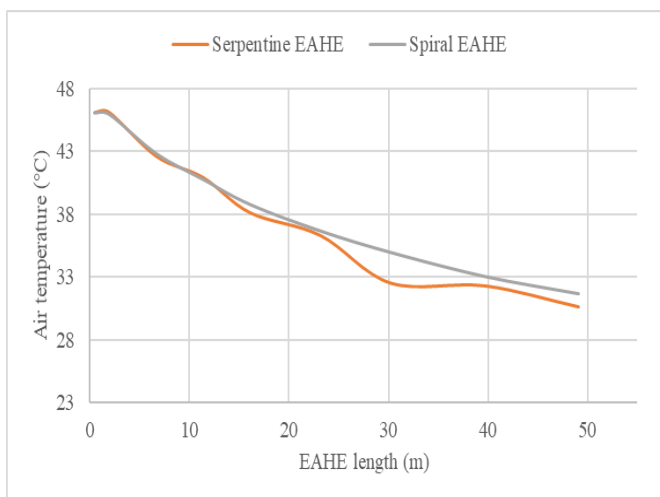
**Figure 17.** Air temperature throughout the EAHE for two designs (flow rate =250 m³/h)

Figure 18. Pressure losses throughout the EAHE designs (flow rate =200 m³/h)

Figure 19. Pressure losses throughout the EAHE designs (flow rate =250 m³/h)

To investigate the higher-pressure losses observed in the serpentine design compared to the spiral design, Figures 20, 21, 22, and 23 illustrate the velocity contours for both configurations, providing detailed insights into the flow dynamics.
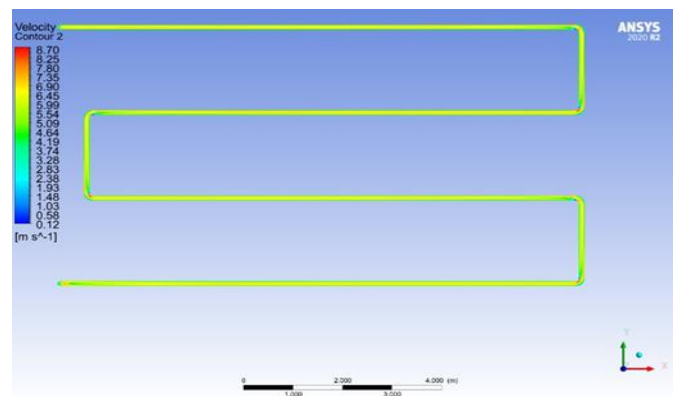
Figure 20. Velocity contour for the serpentine EAHE

The higher-pressure losses in the serpentine design compared to the spiral design are clearly evident in the velocity contours (Figure 20 and Figure 22). The 90° bend (Figure 21) in the serpentine design obstructs the flow, as indicated by the blue regions representing zero velocity in the bend area. This blockage leads to localized high flow

velocities across the bend, this blockage creates localized high flow velocities and agitation in this zone, which slightly improves heat transfer. In contrast, the spiral design facilitates a more uniform flow distribution, as shown by the homogeneous velocity contours throughout the system (Figures 17 and 19), owing to its continuous circulation pattern.
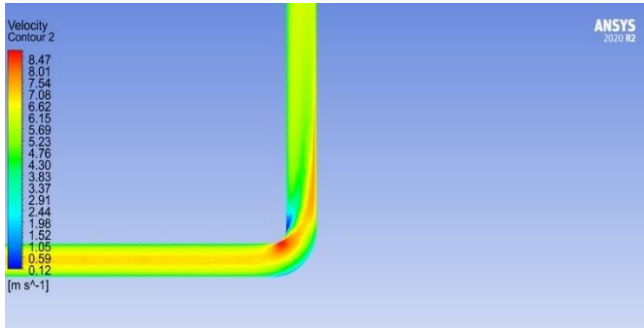

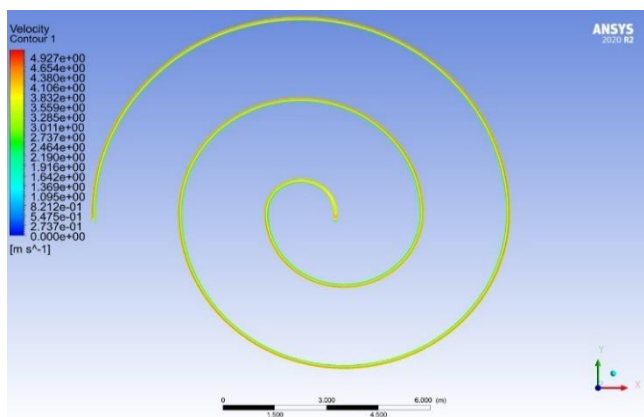**Figure 21.** Velocity contour of the serpentine EAHE at the 90° bend

Figure 22. Velocity contour for the spiral EAHE

Table 7 presents a summary of the performance comparison between the serpentine and spiral EAHE designs, evaluating them under different inlet temperatures and flow rates.

The same trending was observed in Table 7. For example, at an inlet temperature of 42.9°C and a flow rate of 130 m³/h, the serpentine EAHE achieves a slightly lower outlet temperature (28.61°C vs. 29°C) with higher pressure losses (124.10 Pa vs. 101.11 Pa). Similarly, at 37°C and 250 m³/h, the serpentine EAHE shows a slight difference in outlet temperature (29.38°C vs. 29.6°C) but incurs higher pressure losses (405 Pa vs. 323 Pa).

To further assess the performance of the two EAHE designs, we will now evaluate them at a depth of 3 meters with an EAHE length of 50 meters. Figures 24 and 25 show the temperature contours of both the soil and EAHE for the serpentine and spiral designs.
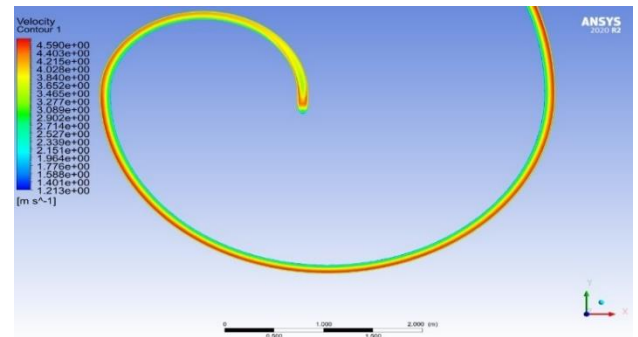

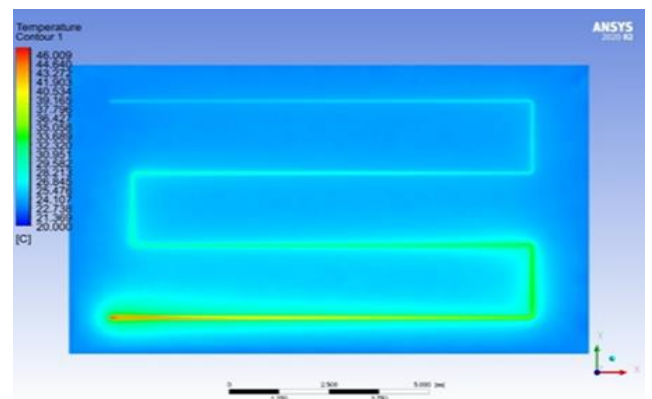**Figure 23.** Velocity contour of the spiral EAHE in the circulation zone

Figure 24. Isothermal contours of soil and serpentine EAHE horizontal path at 3 m depth
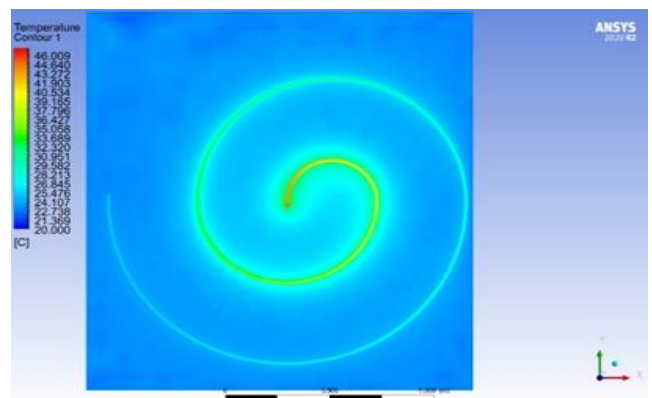
Figure 25. Isothermal contours of soil and spiral EAHE horizontal path at 3 m depth

Table 7. Performance comparison of serpentine and spiral EAHE designs at 2 meters depth

Inlet Temperature (°C)	Flow Rate m³/h	Serpentine EAHE		Spiral EAHE	
		Outlet Temperature (°C)	Pressure Loss (pas)	Outlet Temperature (°C)	Pressure Loss (pas)
46.1	130	28.37	124.10	29.39	101,11
	200	29.95	270.55	30.45	218
	250	30.66	405	31.25	323
42.9	130	28.61	124.10	29	101.11
	200	29.58	270.55	30	218
	250	30.29	405	30.99	323
37	130	28.37	124.10	28.45	101.11
	200	28.95	270.55	29.1	218
	250	29.38	405	29.6	323

Figures 24 and 25 illustrate the soil's cooling effect on the air at a depth of 3 meters, showing temperature variations along the EAHE and surrounding soil through color gradients

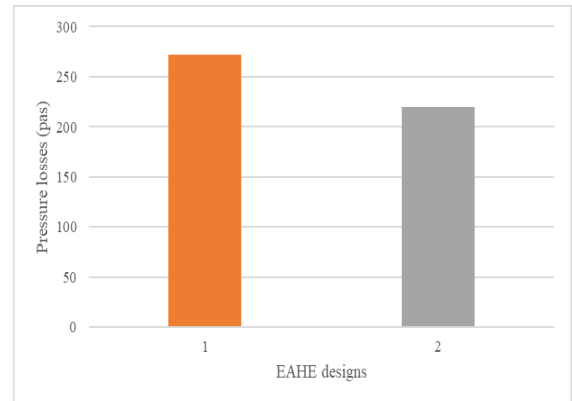The following figures compare the performance of serpentine and spiral EAHE designs at a depth of 3 meters, with an inlet temperature of 46.1°C and flow rates of 130, 200, and 250 m³/h, showing the air temperature distribution and pressure losses for each design at each flow rate.
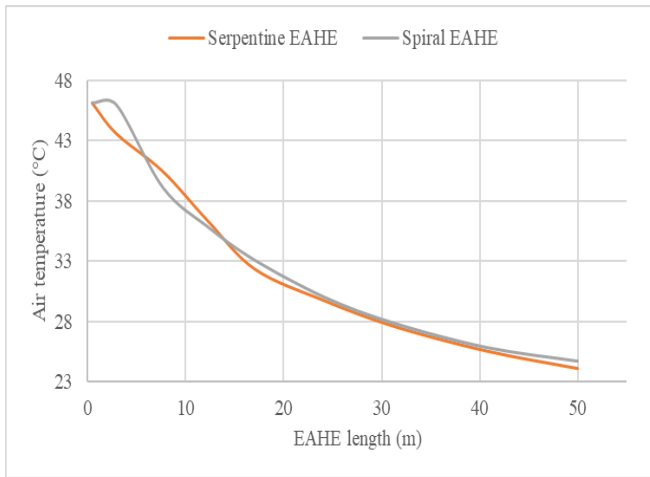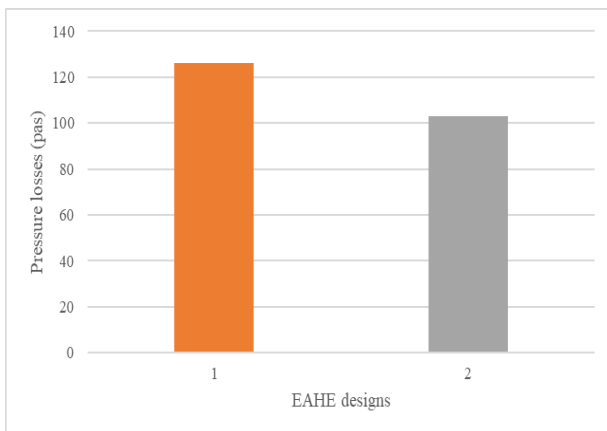

Figure 26. Air temperature throughout the EAHE for two designs (flow rate =130 m³/h)

Figure 27. Pressure losses throughout the EAHE designs (flow rate =130 m³/h)

Figure 28. Air temperature throughout the EAHE for two designs (flow rate =200 m³/h)

The previous figures demonstrate the performance comparison of serpentine and spiral EAHE designs at a depth of 3 meters, with an inlet temperature of 46.1°C and flow rates of 130, 200, and 250 m³/h. Similar trends to those observed at a depth of 2 meters are noted, with slight differences in outlet temperatures and pressure losses for each design at the given flow rates. Specifically:

At 130 m³/h, the serpentine EAHE achieves a slightly lower outlet temperature of 24.08°C compared to the spiral EAHE at 24.76°C (Figure 26). However, the serpentine design incurs a higher-pressure loss of 126 Pa, compared to 103 Pa for the spiral design (Figure 27).

Figure 29. Pressure losses throughout the EAHE designs (flow rate =200 m³/h)

Figure 30. Air temperature throughout the EAHE for two designs (flow rate =250 m³/h)

Figure 31. Pressure losses throughout the EAHE designs (flow rate =250 m³/h)

At 200 m³/h, the serpentine EAHE results in an outlet temperature of 26.01°C, which is slightly lower than the 26.51°C for the spiral EAHE (Figure 28). The pressure loss for the serpentine design is higher at 272 Pa, while the spiral design has a pressure loss of 220 Pa (Figure 29).

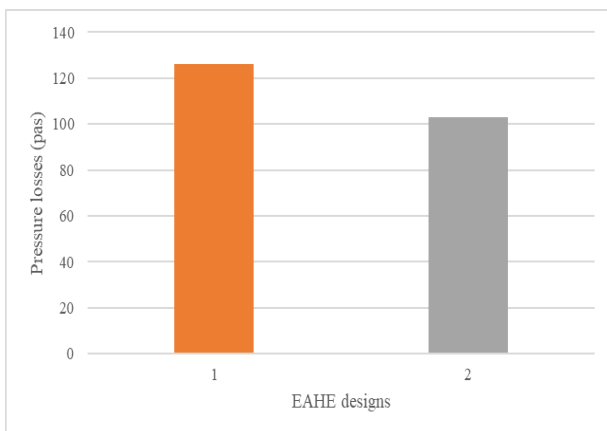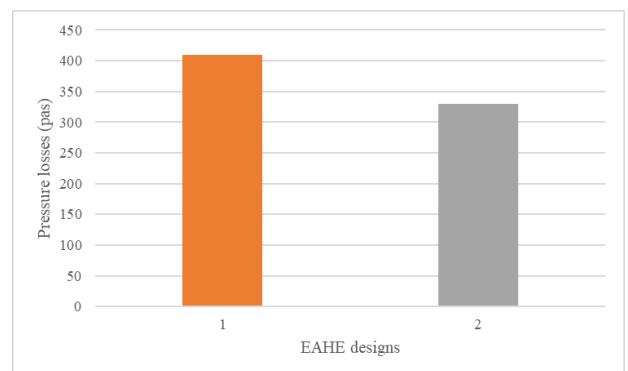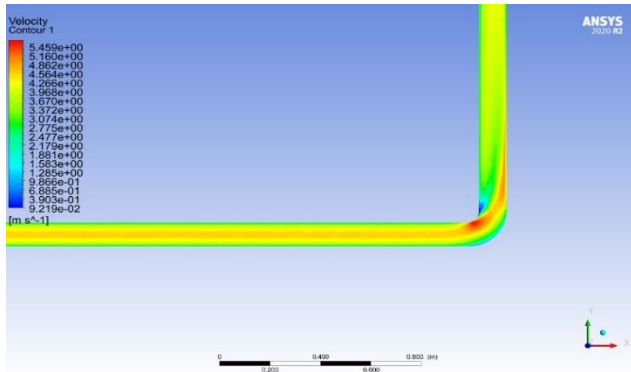At 250 m³/h, the serpentine EAHE shows an outlet temperature of 27.14°C, which is again slightly lower than the spiral EAHE's outlet temperature of 27.68°C (Figure 30). The pressure loss for the serpentine design is higher at 409 Pa, while the spiral design experiences a lower pressure loss of 330 Pa (Figure 31).


Figure 32. Velocity contour of the serpentine EAHE at the 90° bend

To explain the higher-pressure losses observed in the serpentine design, Figures 32 and 33 illustrate the velocity contours for both the serpentine and spiral EAHE designs at a depth of 3 meters. Figure 32 shows the 90° bend in the serpentine design were sharp turns cause flow separation and turbulence, leading to higher pressure losses. In contrast, Figure 33 depicts the circulation zone in the spiral design, where the smooth curve promotes laminar flow, resulting in lower pressure losses.

Table 8 presents a summary of the performance comparison between the serpentine and spiral EAHE designs, evaluating them under different inlet temperatures and flow rates.

As shown in Table 8, similar to the results at 2 meters depth, the serpentine EAHE consistently produces slightly lower outlet temperatures than the spiral EAHE, but with higher pressure losses. For example, at 46.1°C and 130 m³/h, the serpentine has an outlet temperature of 24.08°C and a pressure loss of 126 Pa, while the spiral EAHE reaches 24.76°C with a lower pressure loss of 103 Pa. This trend is consistent across all inlet temperatures and flow rates.
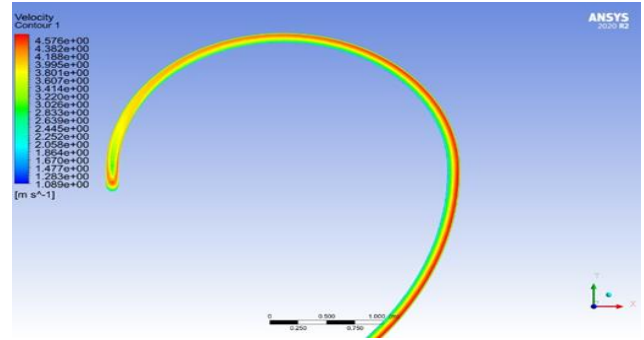
Figure 33. Velocity contour of the spiral EAHE in the circulation zone

Comparing Tables 7 and 8, we observe that at a depth of 2 meters, the comfort temperature has not yet been reached, with the lowest recorded outlet temperature being 28.37°C at an inlet temperature of 37°C and a flow rate of 130 m³/h. In contrast, at a depth of 3 meters, the outlet temperatures fall within the comfort range of 23-26°C for summer, as recommended by ASHRAE [24]. Therefore, the next section will focus on evaluating the two EAHE designs at a depth of 3 meters, with different lengths considered to further assess their performance.

Table 8. Performance comparison of serpentine and spiral EAHE designs at 3 meters depth

Inlet Temperature (°C)	Flow Rate m³/h	Serpentine EAHE		Spiral EAHE	
		Outlet Temperature (°C)	Pressure Loss (pas)	Outlet Temperature (°C)	Pressure Loss (pas)
46.1	130	24.08	126	24.76	103
	200	26.01	272	26.51	220
	250	27.14	409	27.68	330
42.9	130	24.26	126	24.55	103
	200	25.60	272	26.02	220
	250	26.56	409	27.03	330
37	130	23.89	126	24.09	103
	200	24.83	272	25.12	220
	250	25.51	409	25.83	330

Table 9. Performance comparison of serpentine vs. spiral EAHEs at 3 m depth and 35 m length

Inlet Temperature (°C)	Flow Rate m³/h	Serpentine EAHE		Spiral EAHE	
		Outlet Temperature (°C)	Pressure Loss (pas)	Outlet Temperature (°C)	Pressure Loss (pas)
46.1	130	28.02	79.88	27.73	72.63
	200	30.63	173	30.26	157.23
	250	32.08	258	31.72	234.28
42.9	130	27.38	79.88	27.09	72.63
	200	29.58	173	29.25	157.23
	250	30.83	258	30.51	234.28
37	130	26.09	79.88	25.88	72.63
	200	27.63	173	27.4	157.23
	250	28.5	258	28.28	234.28

Table 10. Performance comparison of serpentine vs. spiral EAHEs at 3 m depth and 26 m length

Inlet Temperature (°C)	Flow Rate m³/h	Serpentine EAHE		Spiral EAHE	
		Outlet Temperature (°C)	Pressure Loss (pas)	Outlet Temperature (°C)	Pressure Loss (pas)
46.1	130	30.21	77	30.02	61
	200	33.3	181	32.75	130
	250	34.74	257	34.2	196
42.9	130	29.55	77	29.06	61
	200	31.87	181	31.39	130
	250	33.11	257	32.65	196
37	130	27.61	77	27.26	61
	200	29.24	181	28.9	130
	250	30.11	257	29.79	196

Table 8 presents a comparative analysis of the performance of the serpentine and spiral EAHE designs, evaluated at a depth of 3 meters and a length of 35 meters, across different air inlet temperatures and flow rates.

Table 9 shows that across various inlet temperatures and flow rates. Both designs show similar results, with minor differences. For example, at 46.1°C and 130 m³/h, the serpentine EAHE achieves an outlet temperature of 28.02°C with 72.63 Pa pressure loss, while the spiral reaches 27.73°C with 79.88 Pa. Overall, the spiral provides slightly cooler outlet temperatures but at a slightly lower pressure loss, indicating comparable performance between the designs.

With a length of 26 meters, Table 10 compares the performance of the serpentine and spiral heat exchangers at a depth of 3 meters.

Table 10 shows almost identical heat performance between the serpentine and spiral EAHE designs. For example, at 46.1°C and 130 m³/h, the serpentine EAHE reaches an outlet temperature of 30.21°C with a pressure loss of 77 Pa, while the spiral EAHE reaches 30.02°C with a pressure loss of 61 Pa. Both designs exhibit similar heat transfer performance, with the primary difference being the pressure loss, where the spiral design offers a slight advantage due to its ability to promote more turbulence and maintain fluid continuity over short distances, while the serpentine design experiences higher pressure losses, especially at 90° bends.

5. CONCLUSION

In this study, the numerical simulation of Earth-Air Heat Exchanger (EAHE) designs validated against experimental results for the serpentine and numerical results for the spiral configuration demonstrates the reliability and accuracy of our models. By comparing our simulation outcomes with prior studies, we confirmed that both the serpentine and spiral EAHE configurations accurately represent real world thermal performance under varied conditions.

For a depth of 2 meters with a length of 49 meters, our results show that neither design could achieve the ASHRAE-recommended comfort range (23-26°C) for summer cooling. Although the serpentine EAHE achieved a slightly lower outlet temperature (28.37°C) than the spiral design (29.3°C). This highlights the limitations of 2 meters depth for optimal cooling.

At a depth of 3 meters and a length of 50 meters, both EAHE designs achieved substantial cooling, with outlet temperatures reaching within the comfort range. The serpentine EAHE showed marginally better cooling, achieving 24.08°C compared to 24.76°C for the spiral, but incurred higher

pressure losses. This depth and length combination proved effective for summer cooling.

For the 3-meter depth and 35-meter length, the designs exhibited moderate performance with minimal temperature differences, approaching the comfort range under specific conditions. The spiral EAHE displayed slightly lower pressure losses due to its smoother flow path, which makes it suitable for installations prioritizing energy efficiency over maximum cooling.

Finally, at a depth of 3 meters and a length of 26 meters, both designs demonstrated limited cooling capacity, achieving outlet temperatures slightly above the comfort threshold. Here, the spiral design performed more efficiently with lower pressure losses, indicating a slight advantage in shorter configurations.

Overall, the two EAHE designs serpentine and spiral performed very closely when evaluated at the same lengths. Despite slight differences in outlet temperatures and pressure losses, the overall cooling effectiveness was similar, indicating that both designs can effectively achieve comparable thermal performance under the same length and depth conditions.

The findings emphasize the importance of balancing heat exchange efficiency with operational factors like pressure drop when selecting the optimal EAHE design. Practical applications of these findings can be seen in the design of HVAC systems, geothermal energy systems, and agricultural ventilation, where maintaining an optimal temperature and minimizing energy consumption are critical. Future work could focus on further optimizing these designs by exploring multi-stage configurations, which may enhance overall efficiency. Additionally, efforts could be directed toward improving heat transfer by introducing obstacles or augmenting the surface area, particularly in systems with shorter lengths, where there is significant potential for enhancing heat exchange performance.

REFERENCES

[1] Intergovernmental Panel on Climate Change (IPCC). (2023). Climate change 2022: Mitigation of climate change – working group III contribution to the sixth assessment report of the intergovernmental panel on climate change. Cambridge University Press, Cambridge, UK. https://www.ipcc.ch/report/ar6/wg3/downloads/report/IPCC_AR6_WGIII_FullReport.pdf, accessed on Sep. 3, 2024.

[2] Sonelgaz. (2024). Press release: Record peak demand for electricity on July 21.

https://www.sonelgaz.dz/media/file/2233/21_joyly_202 4_669d29e2b17a03.42802169.pdf, accessed on Nov. 3, 2024.

[3] de Andrade, I.R., dos Santos, E.D., Zhang, H., Rocha, L.A.O., Razera, A.L., Isoldi, L.A. (2024). Multi-objective numerical analysis of horizontal rectilinear earth–air heat exchangers with elliptical cross section using constructal design and TOPSIS. Fluids, 9(11): 257. https://doi.org/10.3390/fluids9110257

[4] Hummood, E., Hasan, M.I., Abd, G. (2024). Investigating the effects of disturbed soil thickness on the performance of Earth-Air Heat Exchanger. International Journal of Heat and Technology, 42(3): 1101-1110. https://doi.org/10.18280/ijht.420337

[5] Xiao, J.X., Li, J.M. (2024). Influence of different types of pipes on the heat exchange performance of an earth-air heat exchanger. Case Studies in Thermal Engineering, 55: 104116. https://doi.org/10.1016/j.csite.2024.104116

[6] Molina-Rodea, Ricardo, Wong-Loya, J.A., Pocasangre-Chávez, H., Reyna-Guillén, J. (2024). Experimental evaluation of a "U" type earth-to-air heat exchanger planned for narrow installation space in warm climatic conditions. Energy and Built Environment, 5(5): 772-786. https://doi.org/10.1016/j.enbenv.2023.06.004

[7] Mostafaeipour, A., Goudarzi, H., Khanmohammadi, M., Jahangiri, M., Sedaghat, A., Norouzianpour, H., Chowdhury, S., Techato, K., Issakhov, A., Almutairi, K., Dehshiri, S.J.H. (2021). Techno-economic analysis and energy performance of a geothermal earth-to-air heat exchanger (EAHE) system in residential buildings: A case study. Energy Science & Engineering, 9(10): 1807-1825. https://doi.org/10.1002/ese3.952

[8] Zajch, A., Gough, W.A., Chiesa, G. (2020). Earth–air heat exchanger geo-climatic suitability for projected climate change scenarios in the Americas. Sustainability, 12(24): 10613. https://doi.org/10.3390/su122410613

[9] Nettari, M., Kaddour, A., Benbelgacem, K., Ikumapayi, O.M., Bezari, S., Al-Dujaili, A.Q., Hebbal, B., Abdulkareem, A.I., Humaidi, A.J., Lorenzini, G., Menni, Y. (2023). Numerical assessment of EAHE systems for refreshment in desert Algerian regions. International Journal of Design & Nature and Ecodynamics, 18(3): 501-508. https://doi.org/10.18280/ijdne.180301

[10] Sakhri, N., Osra, O.A., Alsaygh, F.S., Almutery, S.B., Menni, Y. (2023). Optimizing indoor thermal comfort with wind towers and earth to air heat exchangers: A sustainable solution for energy-efficient housing. International Journal of Low-Carbon Technologies, 18: 915-928. https://doi.org/10.1093/ijlct/ctad084

[11] Roger, S.A.W., Merlin, A.Z., Philippe, O.M., Ruben, M. (2021). Experimental study of heat transfer in a reduced model of bioclimatic air-soil exchanger. International Journal of Heat and Technology, 39(6): 1828-1834. https://doi.org/10.18280/ijht.390617

[12] Ahmad, S.N., Prakash, O. (2020). Optimization of earth air tube heat exchanger for cooling application using Taguchi technique. International Journal of Heat and Technology, 38(4): 854-862. https://doi.org/10.18280/ijht.380411

[13] Moummi, N., Benfateh, H., Hatraf, N., Moummi, A., Ali. (2010). Geothermal cooling: Theoretical and experimental study at the Biskra site. Revue des Énergies Renouvelables, 13: 399-406. https://doi.org/10.54966/jreen.v13i3.208

[14] Benrachi, N., Ouzzane, M., Smaili, A., Lamarche, L., Badache, M., Maref, W. (2019). Numerical parametric study of a new earth-air heat exchanger configuration designed for hot and arid climates. International Journal of Green Energy, 17(2): 115-126. https://doi.org/10.1080/15435075.2019.1700121

[15] Belloufi, Y., Brima, A., Zerouali, S., Atmani, R., Aissaoui, F., Rouag, A., Moummi, N. (2017). Numerical and experimental investigation on the transient behavior of an Earth Air Heat Exchanger in continuous operation mode. International Journal of Heat and Technology, 35(2): 279-288. https://doi.org/10.18280/ijht.350208

[16] Sehli, A., Hasni, A., Tamali, M. (2012). The potential of earth-air heat exchangers for low energy cooling of buildings in South Algeria. Energy Procedia, 18: 496-506. https://doi.org/10.1016/j.egypro.2012.05.061

[17] Hacini, K., Benatiallah, A., Harrouz, A., Belatrache, D. (2021). Efficiency assessment of an earth-air heat exchanger system for passive cooling in three different regions - the Algerian case. FME Transactions, 49: 1035-1046. https://doi.org/10.5937/fme2104035H

[18] Hadjadj, A., Attia, A., Khechekhouche, A., Naili, N., Bendjenidi, B. (2020). Numerical study of a new earth-air heat exchanger configuration designed for Sahara climates. International Journal of Energetica, 5(1): 22-26. https://doi.org/10.47238/ijeca.v5i1.116

[19] Xamán, J., Hernández-Pérez, I., Arce, J., Álvarez, G., Ramírez-Dávila, L., Noh-Pat, F. (2014). Numerical study of earth-to-air heat exchanger: The effect of thermal insulation. Energy and Buildings, 85: 356-361. https://doi.org/10.1016/j.enbuild.2014.09.064

[20] Congedo, P.M., Lorusso, C., De Giorgi, M.G., Marti, R., D'Agostino, D. (2016). Horizontal air-ground heat exchanger performance and humidity simulation by computational fluid dynamic analysis. Energies, 9(11): 930. https://doi.org/10.3390/en9110930

[21] Infoclimat. Monthly climate data for Laghouat – January 2023. https://www.infoclimat.fr/climatologie-mensuelle/60545/janvier/2023/laghouat.html, accessed on July 2024.

[22] Kusuda, T., Achenbach, P.R. (1965). Earth temperature and thermal diffusivity at selected stations in the United States. Report No. 8972, National Bureau of Standards, Washington, D.C., USA. https://nvlpubs.nist.gov/nistpubs/Legacy/RPT/nbsreport 8972.pdf.

[23] ANSYS Inc., ANSYS Europe Ltd. (2020). ANSYS fluent user's guide. Release 2020 R2. July 2020. https://www.scribd.com/document/478910198/ANSYS-Fluent-Tutorial-Guide-2020-R2-pdf.

[24] ASHRAE. (2020). ASHRAE standard 55: Thermal environmental conditions for human occupancy. American Society of Heating, Refrigerating and Air-Conditioning Engineers. https://www.ashrae.org/file%20library/technical%20res ources/standards%20and%20guidelines/standards%20a ddenda/55_2020_a_20210430.pdf.environmental.

NOMENCLATURE

Cp	Pipe thermal specific heat, kJ.kg^{-1}.°C^{-1}
Cs	Soil thermal specific heat, kJ.kg^{-1}.°C^{-1}
D	Pipe diameter, m

ΔP	Frictional pressure loss, Pa	V	Flow velocity of the fluid, $m.s^{-1}$
ΔPs	Singular (or minor) pressure loss, Pa	z	Pipe buried depth, m
f	Darcy-Weisbach friction factor		
K	Loss coefficient	**Greek symbols**	
L	Length of the pipe or duct m		
T_{max}	Maximum ambient temperature, ℃	λ_p	Pipe thermal conductivity, $W/m^{-1}.℃^{-1}$
	Minimum ambient temperature, ℃	ρ	Density of the fluid, $kg.m^{-3}$
T_{mean}	Mean annual temperatur, ℃	ρs	Soil density, $kg.m^{-3}$
$T_{soil}(z,t)$	Soil temperature at depth z and time t, ℃	μ	Viscosity, $kg.m^{-1}.s^{-1}$
Q_v	Air volume rate, $m^3.h^{-1}$	ϕ	Viscous distribution ratio